Available online at www.sciencedirect.com
ScienceDirect
C. R. Physique 9 (2008) 608–623
COMPTES RENDUS PHYSIQUE
http://france.elsevier.com/direct/COMREN/

Synchrotron x-rays and condensed matter/Rayonnement X synchrotron et matière condensée

High-resolution inelastic x-ray scattering to study the high-frequency atomic dynamics of disordered systems

Giulio Monaco

European Synchrotron Radiation Facility, BP220, 38043 Grenoble, France

Available online 14 January 2008

Abstract

The use of momentum-resolved inelastic x-ray scattering with meV energy resolution to study the high-frequency atomic dynamics in disordered systems is here reviewed. The typical realization of this experiment is described together with some common models used to interpret the measured spectra and to extract parameters of interest for the investigation of disordered systems. With the help of some selected examples, the present status of the field is discussed. Particular attention is given to those results which are still open for discussion or controversial, and which will require further development of the technique to be fully solved. Such an instrumental development seems nowadays possible at the light of recently proposed schemes for advanced inelastic x-ray scattering spectrometers. ***To cite this article: G. Monaco, C. R. Physique 9 (2008).***

Résumé

Diffusion inélastique de rayons X à haute résolution pour l'investigation de la dynamique atomique de haute fréquence dans les systèmes désordonnés. Nous passons ici en revue l'utilisation de la diffusion inélastique de rayons X résolue en impulsion et à haute résolution en énergie (meV) pour l'étude de la dynamique atomique haute fréquence dans les systèmes désordonnés. Nous décrivons la mise en œuvre typique de cette expérience, ainsi que quelques modèles couramment utilisés pour l'interprétation des spectres expérimentaux et l'extraction de paramètres pertinents dans l'étude de ces systèmes. Sur la base d'exemples expérimentaux concrets, nous discutons l'état de l'art de cette technique. Nous nous focalisons tout particulièrement sur un certain nombre de questions ouvertes et autres résultats encore controversés, dont l'interprétation définitive nécessitera des développements techniques ultérieurs. Nous montrons finalement qu'à la lumière des récentes propositions pour la réalisation de spectromètres avancés dédiés à la diffusion inélastique des rayons X, ces développements semblent être à notre portée. ***Pour citer cet article : G. Monaco, C. R. Physique 9 (2008).***

Keywords: Inelastic X-ray scattering; Disordered systems

Mots-clés : Diffusion inélastique de rayons X ; Systèmes désordonnés

E-mail address: gmonaco@esrf.fr.

1631-0705/$ – see front matter
doi:10.1016/j.crhy.2007.10.017

1. Introduction

The energy spectrum measured in an off-resonance scattering process of x-rays from matter is basically proportional, at least up to energies of some hundreds of meV, to the atomic dynamic structure factor, $S(q, E)$, where q and E are the momentum and the energy exchanged in the scattering process, respectively. The momentum-resolved technique used to measure this spectrum with meV energy-resolution in the 1–100 nm^{-1} q-range is often referred to as high-resolution inelastic x-ray scattering (IXS), and this is the definition used hereafter.

Formally, $S(q, E)$ is the space and time Fourier transform of the atomic density–density correlation function. This is a key observable in the investigation of atomic dynamics: it holds, in particular, the information on the phonon dispersion relations in crystals, on the acoustic excitations in disordered systems, and on diffusive processes in gases and liquids. Traditionally, the atomic $S(q, E)$ is measured in inelastic light and neutron scattering experiments. In Brillouin light scattering experiments (BLS), due to the small wavevector of visible photons ($k_0 \sim 10^{-2}$ nm^{-1}), only the $q \to 0$ limit is basically probed, corresponding to the Γ point in the reciprocal space of a crystal. Inelastic neutron scattering (INS) experiments complement light scattering ones by probing a finite q range, which in particular allows for the measurement of the full phonon dispersion curves in a crystal. This possibility is disclosed to neutron scattering by the fact that the energy of neutrons with wavelengths of the order of inter-particle distances is $\sim$100 meV, i.e. quite close to the typical energies of phonons in crystals. Consequently, a neutron spectrometer with a moderate relative energy resolution offers an easy access to the atomic dynamics. Different is the case of x-rays: for example, x-rays with a wavevector of 1 Å^{-1} have an energy of $\sim$10 keV. Consequently, in order to detect the energy exchanged by an x-ray beam with an acoustic phonon, a resolving power of at least 10^6 is needed. For this technical difficulty, x-rays have not been considered useful in the study of the atomic dynamics until only recently.

Things have changed considerably since the advent of synchrotron radiation sources, which have provided brilliant x-ray beams amenable for experiments fulfilling such pushed resolving power requests. The first IXS experiment with 55 meV energy resolution was set up during the years 1984–1987 at the second generation synchrotron source of Doris II, Hamburg, and lead to the first IXS measurement of the acoustic phonon dispersion curve in a crystal [1]. Important advances in the technique came few years later with the advent of the third generation synchrotron source of the ESRF, that started to deliver an x-ray beam with an unprecedented brilliance. Exploiting the beam quality, and using new ideas in perfect crystal optics, a new instrument was build up during the years 1992–1996 at the beamline ID16 of the ESRF by F. Sette and co-workers [2–4], capable of achieving a 1.5 meV energy resolution with an intensity still exploitable for experiments. Since then, the IXS technique has seen continuous improvements in terms of flux, flexibility and stability that push further and further its scientific case.

The (q, E) region of interest for the study of the acoustic excitations in disordered systems currently covered by the IXS technique is shown in Fig. 1 (black border) together with the regions accessible to Brillouin light and ultra-violet scattering (blue border) and to INS (green border). In Fig. 1 the (q, E) region foreseen to be accessible to IXS using improved optical schemes [5] is shown as well (red border).

Nowadays, IXS can be considered as an established tool to measure the atomic $S(q, E)$, in a few cases extending and, more generally, complementing INS techniques. In fact, though IXS and INS probe the same atomic dynamics, the measured spectra are differently modulated by different atomic species, the weight function being the atomic form factor $f(q)$ for IXS and the scattering length b for INS. Thus, the study of the atomic dynamics of a polyatomic system profits from the joint use of IXS and INS just in the same way as a structural study profits from a joint use of x-ray and neutron diffraction. Moreover, though IXS presents several disadvantages with respect to INS, it has as well some important advantages which define a class of experiments where IXS really extends the INS capabilities. The most relevant disadvantages of IXS with respect to INS are readily listed:

(i) The best energy resolution achieved in IXS experiments is $\sim$1 meV, while INS experiments can easily do much better. Though there exist optical schemes to push the IXS resolution below 1 meV [5], their feasibility has not been demonstrated yet.
(ii) The rapid decrease of $f(q)$ with q makes IXS experiments very difficult already for q larger than few Å^{-1}, while there is no such stringent limitation in INS experiments.
(iii) Neutrons can be scattered both coherently and incoherently, the first channel probing $S(q, E)$ and the second its self part, which gives a direct handle on single atom dynamics; x-rays miss such richness, and only probe $S(q, E)$.

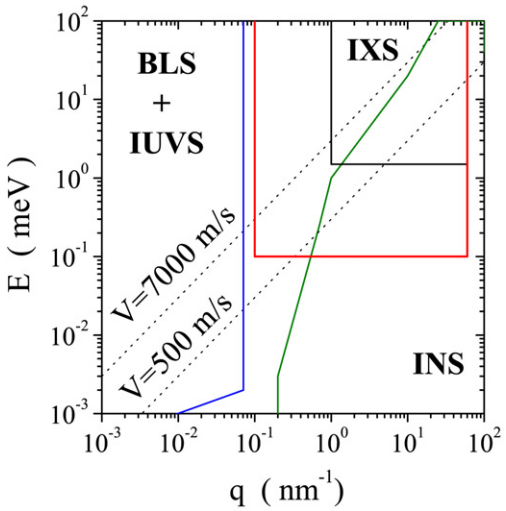

Fig. 1. The wavenumber (q) and energy (E) space for the acoustic excitations in first Brillouin zone as covered by different techniques: Brillouin light scattering (BLS) together with its extension to the ultraviolet regime (IUVS); inelastic neutron scattering (INS); inelastic x-ray scattering (IXS) in the range that is presently covered (black border) and foreseen to be covered in the future (red border). The dashed lines indicate two extreme longitudinal sound velocities for liquids and glasses.

In order to understand where IXS extends INS capabilities, it is as well useful to list the main advantages of IXS over INS:

(i) In a scattering process, the probe cannot create excitations with an energy larger than its own. This simple fact, together with the energy-wavenumber relation for neutrons, sets kinematic limitations for INS – while IXS does not suffer of this problem. In particular, INS has severe difficulties to probe at low-q collective excitations propagating with a speed larger than ∼1500 m/s. This is not a problem in single crystal studies, where it is always possible to probe the same excitations at larger q, in some higher order Brillouin zone; it is, however, a severe limitation in the study of the collective excitations of disordered systems where, due to the lack of translational invariance, these excitations only exist at low-q, in the so-called first pseudo Brillouin zone. This opens a class of scientific problems where IXS significantly extends INS capabilities, with particular reference to the study of the acoustic excitations in liquids and glasses. A similar situation occurs for the study of vibrations in the 100 meV range, and in the study of high-energy optic modes in crystals: INS can access these modes only at high-q, where the energy resolution is no longer optimal or, in the case of liquids, where the vibrational spectrum is often already heavily modified as a consequence of the recoil of the atom struck by the neutron. Here, IXS has the advantage to be able to easily access high energy vibrations at low-q with high-energy resolution.

(ii) X-ray beams, contrary to neutron ones, can easily be focused down to a linear size of ∼10 μm or less. The availability of small beams reduces drastically the problems related to multiple scattering processes, which require sophisticated procedures of data reduction and which are often non-negligible in INS experiments. More importantly, small beams disclose the access to samples of small sizes: samples only available in very small quantities, like crystals difficult to grow to large sizes, or very expensive samples, or also materials subjected to extreme thermodynamic conditions. Within this last class of systems, both crystalline and disordered materials under extreme conditions of pressure and/or temperature represent an area of growing interest.

(iii) The absence of incoherent scattering, previously listed as a disadvantage, is at the same time an advantage of IXS over INS since it simplifies the cross-section and makes the IXS access to $S(q, E)$ sometimes more direct that the INS one. This is particularly important in line-shape studies of $S(q, E)$ in disordered systems.

It is finally important to underline that IXS with meV energy resolution, due to the above mentioned reasons, has gained an important place among the synchrotron radiation activities worldwide. Today, at the ESRF, the beamline ID28 [6] is fully dedicated to it, and beamline ID16 [7] for ∼60% of its time; at the Advanced Photon Source in Chicago – the 7 GeV synchrotron radiation source in the USA – one beamline (ID3) carries on IXS experiments

with meV energy resolution [8], and a new beamline fully dedicated to this activity is under commissioning and is expected to be fully operational in 2007; at SPring-8 – the 8 GeV national Japanese synchrotron radiation source – one beamline (BL35XU) is fully dedicated to this activity [9]. Moreover, a new IXS beamline is under study at the new synchrotron radiation source of NSLS-II at Brookhaven, in the USA.

This article is meant to provide a short review of IXS studies of the high-frequency atomic dynamics in disordered systems and is organized as follows. Section 2 summarizes the main technical solutions presently adopted for IXS experiments. Section 3 recalls the models most commonly used to interpret the experimental spectra. In Section 4 some selected recent results on the high-frequency atomic dynamics of disordered systems are overviewed. Some general conclusions are finally reported in Section 5.

2. The high-resolution inelastic x-ray scattering experiment

High-resolution inelastic x-ray scattering experiments are presently feasible at all three existing high-energy third generation synchrotron sources ESRF, APS and SPring-8. The way these experiments are realized in these different centers is very similar, and in what follows the experimental realization at beamline ID16 of the ESRF will be discussed as an example.

The optical layout of beamline ID16 in the high-resolution configuration for atomic dynamics studies is shown in Fig. 2. Schematically, the x-ray beam is monochromatized in two steps (premonochromator, monochromator) and then focused at the sample stage; the radiation scattered by the sample is collected at a chosen scattering angle and analyzed in energy by the spectrometer, basically consisting of a crystal analyzer and a detector. Energy spectra are collected by scanning the energy of the incident beam – this is accomplished by scanning the temperature of the monochromator crystal with respect to that of the analyzer crystal.

The experimental strategy used for IXS measurements with meV energy resolution resembles that of a triple axis neutron spectrometer, where the first axis selects the incident photon energy (backscattering monochromator), the second one selects the scattering angle (sample goniometer), and the third axis selects the scattered photon energy (analyzer crystal).

In more detail, the x-ray beam is provided by three undulators with a magnetic period in the range of 26–35 mm and with a total length of 4.8 m. The x-ray beam from the undulators odd harmonics has a spectral bandwidth $\Delta E/E \sim 10^{-2}$, an angular divergence of approximately 40×20 μrad^2 ($H \times V$) FWHM, and an integrated power within this divergence of the order of ∼300 W. A set of cylindrical compound refractive lenses, made out of beryllium, are used to collimate the beam in the vertical direction to better than 2 μrad with a transmission higher than 90%.

The undulator beam is premonochromatized to a bandwidth $\Delta E/E \sim 10^{-4}$ using a pair of independent Si(1,1,1) crystals cooled using liquid nitrogen to evacuate the heat load of the incoming beam.

The premonochromatic beam is further monochromatized using a Si crystal operated in near backscattering geometry (Bragg angle $\vartheta_B = 89.98°$, asymmetry angle $\alpha = 85°$ in the dispersive vertical plane) and on a high reflection order. The backscattering geometry is motivated by the requirement that the Darwin width of the reflection of interest be larger than the natural beam divergence. A high order of reflection is required since the higher is the reflection order

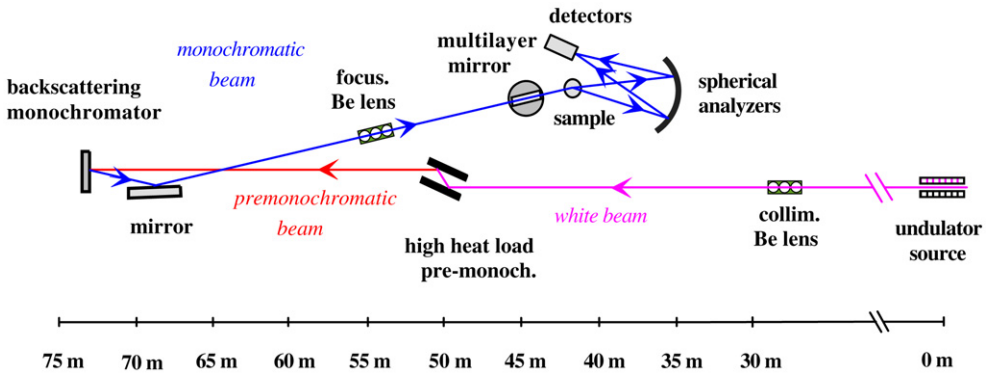

Fig. 2. Optical layout of beamline ID16 at the ESRF in the high-resolution configuration for atomic dynamics studies.

Table 1
Representative values of the measured photon flux of the x-ray beam at the sample stage. n indicates the order of the Si(n, n, n) reflection, and E the corresponding energy in the backscattering configuration. ΔE is the energy bandwidth while ΔE_{tot} is the total (monochromator + analyzer) energy resolution that can be achieved using the 6.5 m long horizontal spectrometer. Flux values refer to a three U35 undulators operation, with 200 mA ring current

n	E [eV]	ΔE [meV]	ΔE_{tot} [meV]	3 × U35 flux [photons/s]
7	13 839	5.3	7.6 ± 0.2	1.0×10^{11}
8	15 816	4.4	5.5 ± 0.2	7.6×10^{10}
9	17 793	2.2	3.0 ± 0.2	2.4×10^{10}
11	21 747	0.83	1.5 ± 0.1	4.6×10^{9}
12	23 724	0.73	1.3 ± 0.1	3.4×10^{9}
13	25 701	0.5	1.0 ± 0.1	1.0×10^{9}

the smaller is the corresponding $\Delta E/E$. In fact, for a given Bragg reflection $\Delta E/E$ is basically inversely proportional to the number of reflecting crystalline planes throughout the extinction length of the x-ray beam, and the extinction length in turn increases with increasing energy or reflection order [5], see Table 1. At the same time, a higher order of reflection means a lower diffracted intensity, and a compromise has to be found between resolution and intensity.

Depending on the experiment, reflection orders between the Si(7,7,7) and the Si(13,13,13) are typically chosen, which correspond to energy bandwidths between 5 and 0.5 meV, see Table 1. Reflection orders higher than the Si(13,13,13) provide one with a beam flux at the sample stage $<10^9$ photons/s, a value that, with current optics and detectors, is too small to allow performing successful IXS experiments. The monochromator crystal is temperature controlled at the mK level by a high precision thermometry bridge in closed-loop operation with a PID controlled heater unit.

The focusing of the beam at the sample position can be provided by different optical schemes which lead to focal spot typically comprised between $40 \times 60\ \mu\text{m}^2$ and $250 \times 100\ \mu\text{m}^2$ ($H \times V$) FWHM. The former figures refer to the use of a cylindrical graded multilayer to provide horizontal focusing, while the latter ones refer to the simplest available optical scheme based on the use of a single Pt-coated toroidal mirror located 4 m away from the backscattering monochromator. Representative values of the measured photon flux of the x-ray beam at the sample stage in the setup where the toroidal mirror provides the focusing are reported in Table 1.

The photons scattered by the sample are collected using a 6.5 m long horizontal spectrometer. They are energy-analyzed by five spherical analyzers mounted in the horizontal spectrometer and which operate similarly to the high-resolution monochromator (i.e. in a near-backscattering configuration and at the same reflection order as the backscattering monochromator). These analyzers focus the energy-analyzed photons onto five independent Si-diode detectors installed close to the sample position. The whole spectrometer arm can be rotated around the sample position in order to select the scattering angle $2\theta_s$ and then the exchanged momentum q, being $q = \frac{4\pi}{\lambda} \sin\theta_s$, where λ is the wavelength of the incoming beam. The analyzers are mounted with a constant angular offset of 1.5°, which corresponds to a basically constant q offset of 3 nm^{-1} at 21 747 eV, the energy corresponding to the Si(11,11,11) Bragg reflection. Five spectra at five different exchanged momentum values – one for each analyzer – can then be collected at the same time for each setting of the horizontal spectrometer arm. The q-resolution, Δq, corresponding to each spectrum is selected by slits mounted in front of the analyzer units. Typical figures are $\Delta q/q \approx 10$–20% for q in the 1–5 nm^{-1} range. Further details on beamline ID16 can be found in Refs. [2–4,7].

3. Models to describe the IXS spectra

The spectrum $I(q, E)$ of a moderately quantum monatomic system[1] measured in a high-resolution IXS experiment can be readily expressed as:

[1] Here I refer to a moderately quantum system as to a system where the quantum effects that arise from the overlap between the single-particle wavefunctions can be neglected. The quantized character of the energy transfers at the microscopic level leads however to a natural unbalance of the spectrum that is expressed by the detailed balance condition that clearly has to be fulfilled.

$$I(q,E) = I_o\big[R(E)\big] \otimes \left[\frac{E}{k_B T}\big(n(E)+1\big)S(q,E)\right], \tag{1}$$

where I_o is an overall intensity factor; $R(E)$ is the instrumental function; $\otimes$ stands for convolution, $n(x) = [\exp(x)-1]^{-1}$ is the Bose factor, with T the temperature, k_B the Boltzmann constant and $x = E/k_B T$; and $S(q,E)$ is the *classical* dynamic structure factor defined as the space and time Fourier transform of the density fluctuations correlation function, $\Phi_q(t)$. An equation of motion for $\Phi_q(t)$ can be written in the form of a generalized Langevin equation [10,11], which leads to the following formal expression for $S(q,E)$:

$$S(q,E) = \frac{2\hbar^2 v_o^2 q^2}{E}\,\mathrm{Im}\big[E^2 - \hbar^2\omega_o(q)^2 - \mathrm{i}Em_q(E)\big]^{-1}, \tag{2}$$

where Im denotes the imaginary part. The parameter $\omega_o(q)$ introduced in Eq. (2) is fixed by the second sum rule for $S(q,E)$ and turns out to be:

$$\omega_o^2(q) = \frac{(qv_o)^2}{S(q)}, \tag{3}$$

where $S(q)$ is the static structure factor and v_o is the classical thermal speed defined in terms of the atomic mass, M, being $v_o^2 = k_B T/M$. Moreover, in Eq. (2) the second memory function, $m_q(E)$, of the so-called Zwanzig–Mori expansion of $S(q,E)$ has been introduced [12]. Alternatively, Eq. (2) can be simply considered as an equation that defines $m_q(E)$. In fact, the real advantage in using Eq. (2) is that the introduction of simple models for $m_q(E)$ – instead than directly for $S(q,E)$ – guarantees that at least the first two non-zero spectral moments of $S(q,E)$ are always fulfilled.

Different models for $m_q(E)$ are utilized in different portions of (q,E) space. Two quantities are usually introduced as reference points in such a space: the average interatomic distance, a, and the characteristic relaxation time for the density fluctuations, τ. The conditions $qa \ll 1$ and $E\tau \ll \hbar$ define the region of the (q,E) space where simple hydrodynamics holds, and in this range an analytical, well-known expression for $m_q(E)$ is available [10]. If condition $\omega\tau \ll 1$ fails and $qa \leqslant 1$, as it occurs for most of the IXS studies, one enters the realm of the so-called molecular hydrodynamics [10]. In this region the atomic dynamics is influenced both by structural and relaxational effects. For what concerns the former, their intervention directly comes into play through the structure factor, $S(q)$. For what concerns the latter, instead, an appropriate model for $m_q(E)$ has to be introduced. In general, the smooth transition from the simple hydrodynamics regime to the molecular one is the main argument used to extend the hydrodynamics description by retaining its formal structure, but replacing the thermodynamic derivatives and the transport coefficients with functions that can vary both in space (or wavenumber) and time (or energy). Within this formalism, the memory function (in time domain) can be written as:

$$m_q(t) = \hbar\omega_o^2(q)\big[\gamma(q)-1\big]\mathrm{e}^{-D_T(q)q^2 t} + K_l(q,t), \tag{4}$$

where $\gamma(q)$ and $D_T(q)$ are q dependent generalizations of the constant pressure to constant volume specific heat ratio $\gamma = C_P/C_V$ and of the thermal diffusion coefficient $D_T = \kappa/(\rho C_P)$, where κ is the thermal conductivity and ρ the mass density and where $K_l(q,t)$ is the q and t dependent generalization of the kinematic longitudinal viscosity ν_l. The strength of the thermal contribution, $\omega_o^2(\gamma-1)$, is typically one order of magnitude smaller than that corresponding to the longitudinal viscosity contribution [10]. Therefore, the most important and delicate point here is to model $K_l(q,t)$. This is usually accomplished using phenomenological expressions that contain the necessary ingredients to describe the atomic dynamics.

The simplest choice for $K_l(q,t)$ is an exponential decay. This choice, which is usually known as the *viscoelastic* model, allows for a reasonably good description of the evolution of $S(q,E)$ with q for $q \approx q_m$, where q_m denotes the first diffraction peak position. However, for $q \approx q_m/10$, i.e. in the standard range for IXS studies of disordered systems, the viscoelastic model begins to fail.[2] This is usually explained by saying that, when decreasing q below q_m, the memory function splits into two contributions. The first one is related to atomic vibrations in the local atomic environment, which induce a loss of correlation usually on the 10^{-13} s time-scale, with almost no temperature dependence. This contribution is often called the microscopic decay. The second contribution is required to describe the

[2] See, for example, Fig. 6.2, page 229 of Ref. [11]. There, the $S(q,E)$ of liquid Cesium ($T = 308$ K) at $q = 6$ nm^{-1} is shown to be only badly described by a single-exponential memory function.

relaxation of the density fluctuations that takes place at longer times characterized by the characteristic time τ, and is usually temperature dependent. This second process generally corresponds to the structural relaxation [13].

As a consequence of this conceptual picture, and beginning with the classical molecular dynamics study by Levesque et al. on the Lennard–Jones liquid near its triple point [14], it is customary to represent the function $K_l(q,t)$ as the sum of two exponentials. The characteristic time of the microscopic decay turns out to be, however, much faster than the characteristic time of the structural relaxation [14]. As a consequence, and in order to use a model with a minimum number of parameters, the microscopic decay is usually represented with a simple Markovian term. As a matter of fact, this simple approximation has been shown to be detailed enough to well represent basically all the available experimental data. Summarizing, in the (q, E) range covered by typical IXS experiments, the minimal expression for $K_l(q,t)$ used in the analysis of the data is the following:

$$K_l(q,t) = 2\hbar\Gamma(q)\delta(t) + \hbar\frac{q^2}{\rho}\Delta^2(q)\mathrm{e}^{-t/\tau(q)}, \tag{5}$$

where $\Gamma(q)$ represents the very fast decaying contribution to $K_l(q,t)$; $\tau(q)$ is the q-dependent time which characterizes the long time tail of $K_l(q,t)$; and $\Delta^2(q)$ is the relaxation strength which is related to two further important quantities, $c_\infty(q)$ and $c_o(q)$, i.e. the q-dependent generalizations of the usual limiting frequency and adiabatic sound speeds, by the relation [15]:

$$\Delta^2(q) = \rho\big[c_\infty^2(q) - c_o^2(q)\big]. \tag{6}$$

In fact, the second term on the right-hand side of Eq. (5) is in principle able to describe the classical phenomenology of the dispersion and absorption of the sound waves, e.g. the transition of the sound speed from its low-frequency, adiabatic value, $c_o(q)$, to the high frequency, limiting value, $c_\infty(q)$ [16]. It is as well useful to recall that the requirement that Eq. (4) correctly extrapolates to the simple hydrodynamics regime imposes the following integral condition:

$$\lim_{q\to 0}\int_0^\infty \mathrm{d}t\; K_l(q,t) = \hbar q^2 \nu_l. \tag{7}$$

Eqs. (4) and (5) simplify considerably when applied to IXS studies of glasses. In fact, in the limits $\gamma \approx 1$ and $E\cdot\tau(q) \gg \hbar$, which are both appropriate for undercooled liquids and glasses probed at the typical IXS energies and wavenumbers, the dynamic structure factor, Eq. (2), reads:

$$\frac{S(q,E)}{S(q)} = (1-f_q)\frac{2\hbar^3\Omega^2(q)\Gamma(q)}{[E^2-\hbar^2\Omega^2(q)]^2 + [\hbar E\Gamma(q)]^2} + f_q\delta(E), \tag{8}$$

where $\Omega(q) = qc_\infty(q)$ and $f_q = 1 - [\omega_o(q)/\omega_\infty(q)]^2$, the latter being known in the literature of glass-forming systems as the non-ergodicity parameter [13]. Eq. (8) is typically used to analyze IXS data, and is known as the *damped harmonic oscillator model* (*DHO*). Its ability to describe the IXS spectra is demonstrated in Fig. 3, where a typical example of an IXS spectrum of a glass is reported (open circles) together with the best fitting equation (8) (full line) and the two distinct elastic and inelastic contributions.

It has finally to be emphasized that the formulation presented here is a generalization of the formalism used at low q, and thus does not take into account the contribution of transverse excitations which are known to appear in the spectra of several systems at high q [17,18]. In fact, this effect becomes relevant at q values sufficiently high that the pure transverse or longitudinal polarization of the modes can no longer be invoked. When such an additional excitation appears in the IXS spectrum, and in the absence of a model able to fully take it into account, the data analysis is usually carried out adding up two DHO contributions [17,19–21].

4. Selected results

4.1. High-frequency sound waves in glasses

Glasses exhibit universal anomalies in their thermal properties – see Ref. [22] for a review and for references to the original papers:

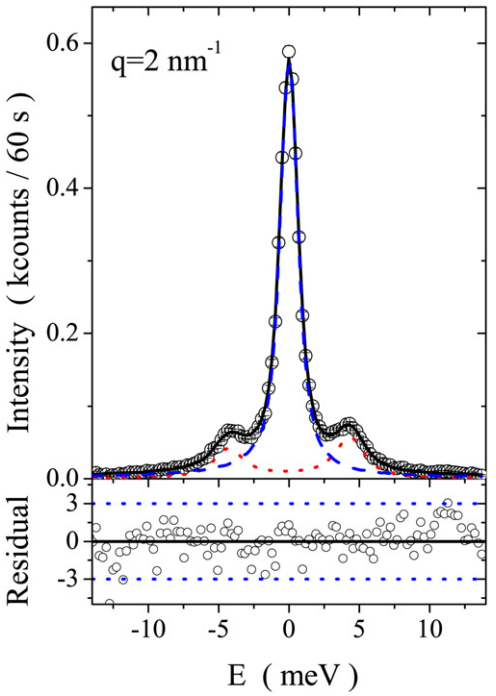

Fig. 3. Upper panel: IXS spectrum of the glass of glycerol at $T = 150$ K and $q = 2$ nm^{-1} (open circles) together with the best fit obtained using the DHO model (full line). The elastic and inelastic contributions derived from this model are shown as well after convolution to the instrumental function (dashed line and dotted line, respectively). Bottom panel: residual of the fit, in standard deviation units. The dashed lines indicate the $\pm 3\sigma$ levels.

(i) The specific heat, C_P, at low temperature is approximately proportional to T and, at $T = 0.1$ K, exceeds that of the corresponding crystals by a factor of $\sim$100. Moreover, at temperatures of the order of 10 K a bump appears in C_P/T^3, which corresponds to an excess of low-frequency modes over the Debye density of vibrational states. This excess of low-frequency modes is also directly observed in the vibrational density of states – which can be measured for example using neutron scattering [23] – and, in that case, is known as the boson peak.

(ii) The thermal conductivity, κ, is much smaller than in the corresponding crystals and nearly proportional to T^2 below 1 K. Moreover, at the same temperatures where C_P/T^3 shows the bump, κ shows a plateau.

These facts contrast with what one would intuitively expect. In a pure dielectric system the low-temperature thermal properties are governed by the behavior of long-wavelength phonons – for example, thermal properties at 1 K are determined by acoustic excitations with wavelengths of $\sim$1000 Å. On such a scale, the regular lattice of a crystal, as well as the irregular network of a glass, should both appear as an elastic continuum. Then, the Debye model which leads to a T^3 law for specific heat and thermal conductivity should be applicable in both cases. This, however, is not observed in glasses.

The origin of these thermal anomalies has been, and still is, studied by looking at the acoustic properties of glasses, and the overall picture which comes out is quite complex and, by today, still not completely understood [24]. These studies explain the low-temperature anomalies in C_P and κ within the so-called tunnelling model [25,26], i.e. by assuming the existence of almost degenerate configurations for small groups of atoms and of quantum tunnelling to permit the atoms to move between the two configurations. This model works formally well to describe the low-frequency acoustic behavior and the low-temperature thermal anomalies up to few K. At temperatures higher than that, and in particular in the $\simeq$10 K region where the plateau in the thermal conductivity and the bump in the specific heat appear, additional universal mechanisms have to be invoked which require to study the acoustic properties in the GHz to THz range. This has triggered a sizeable experimental (e.g. [27,28]), computational (e.g. [29–31]) and theoretical (e.g. [31–33]) research effort which has improved our understanding of the problem but has not fully clarified it yet.

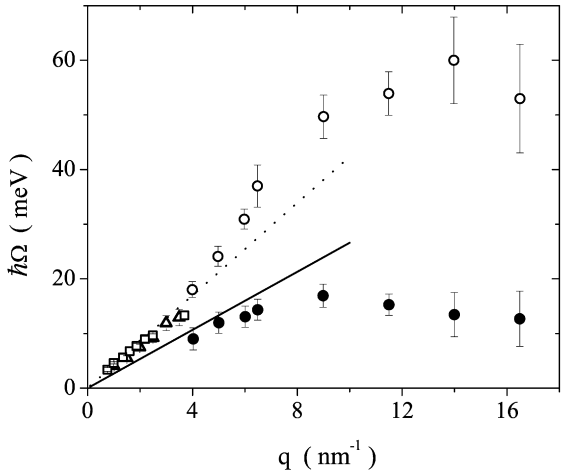

Fig. 4. Dispersion relations in vitreous silica. Open and full circles are experimental data measured at $T = 1270$ K and representing the excitation energies [$\hbar\Omega(q)$] of the longitudinal and transverse branches, respectively [20]. Open triangles and squares correspond to the longitudinal branch – which is the dominating one at low q's – and refer to 1050 K [37] and 1375 K [38], respectively. The dashed and full lines are the extrapolation of the low frequency longitudinal and transverse sound velocity, respectively.

The results obtained by IXS on the acoustic-like excitations of glasses in the THz and sub-THz frequency range are largely sample-independent and can be summarized as follows. The longitudinal acoustic excitations measured for different values of the exchanged momentum q are characterized by a polycrystal-like dispersion of their frequency $\Omega(q)$, with in particular a linear dependence on q up to q values of few nm^{-1} and with a slope corresponding to the limiting longitudinal sound velocity [34]. The maximum q-value up to which it is still possible to observe acoustic excitations is an important information to extract from the experimental spectra. The answer is difficult because, on increasing q, the acoustic excitations become broad and lie on top of the tails of the intense quasi-elastic peak. For this reason, the $S(q, E)$ spectra have been interpreted in quite different, and sometimes contrasting, ways. A typical example of this is represented by the prototypical case of vitreous silica. A possible way to interpret the IXS spectra of permanently densified vitreous silica is by performing the data analysis using a single excitation and by noting that around and above the boson peak position the inelastic contribution can be described by a non-propagating excitation quite similar in shape to the boson peak itself [35]. This interpretation is based on the picture that when the acoustic excitation energy approaches the boson peak position the Ioffe-Regel limit is reached beyond which the concept of propagation for the acoustic modes looses its meaning [36]. A similar picture appears as well in models trying to connect the high-frequency acoustic modes to the thermal conductivity and the specific heat in the $\simeq$10 K temperature region [32]. In a different and contrasting view, it is proposed that the inelastic component at high q is actually the sum of two different excitations. A study of the atomic $S(q, E)$ of vitreous silica – performed on an extended energy range (up to 115 meV) and with a high statistical accuracy – has shown that the longitudinal mode disperses up to quite high energies above the boson peak position and that a second excitation becomes more and more evident in the spectra as q is increased [20], see Fig. 4. This second excitation – in the q range where it is visible – is almost non-dispersing and is assigned to the transverse acoustic branch [20]. These results have been confirmed as well on other glasses [19].

An additional result that goes in this same direction has been obtained by developing a new experimental strategy measuring the atomic $S(q, E)$ in vitreous silica varying the exchanged momentum at fixed energy – instead of scanning the energy at fixed q – thus providing spectra with much better identified inelastic features [39]. In this way direct evidence has been obtained of longitudinal acoustic excitations in vitreous silica at energies above the boson peak one. These results obtained on vitreous silica have then been confirmed on other glasses as well [40].

Another relevant parameter that can be extracted from the analysis of the IXS spectra is the broadening, $\Gamma(q)$, of the acoustic-like excitations since it gives direct information on the high-frequency acoustic absorption. In the q region where the acoustic dispersion relation is linear, the broadening of the acoustic excitations had been found to show a T-independent, q^2 (or Ω^2) behavior up to q values of the order of few nm^{-1} [34]. In particular, no indication of changes of behavior of the longitudinal acoustic modes at the boson peak frequency had been found [27]. It has to be underlined that the Ω^2 behavior found at high frequency does not correspond to that measured at lower frequencies

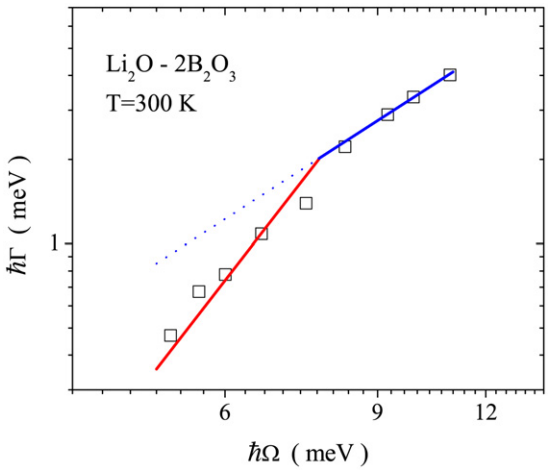

Fig. 5. Dependence of the damping Γ (open squares) of the high-frequency acoustic waves on the wave frequency Ω for the Li_2O–$2B_2O_3$ glass at $T = 300$ K, from Ref. [28]. The full blue line describes the Ω^2 dependence at high energy, and the dashed blue line is its extrapolation at lower energies, where it clearly overestimates the experimental data. The lower energy points are much better described by a Ω^4 law (full red line).

(for example with Brillouin light scattering) and generally ascribed to anharmonicity. In fact, the origin of the acoustic loss mechanism at high-frequency is surely non-dynamic [41] though its exact nature is still being discussed on. One important observation is based on the fact that also a simulated harmonic glass at basically zero-temperature shares the same main features for $\Gamma(q)$ as measured in IXS experiments on real glasses [42], thus pointing to the central role of the topological disorder in the high-q acoustic dynamics. In more recent analyses, the Ω^2 dependence of $\Gamma(q)$ has been explained in terms of spatial fluctuations of the local elastic moduli [43], claiming an even quantitative agreement between the model predictions and the measured experimental values.

Recent experimental results which follow the continuous improvement of the technique and the use of better adapted measuring schemes have, however, shown that at least in permanently densified silica [44] and in the lithium diborate Li_2O–$2B_2O_3$ glass [28] the broadening $\Gamma(q)$ experiences a remarkably rapid increase with Ω (much larger than Ω^2 and compatible with Ω^4) as $\Omega(q)$ approaches the boson peak position from below, see Fig. 5. These results have been interpreted in terms of resonance and hybridization of the acoustic waves with the modes embedded in the boson peak. They do indicate that the longitudinal acoustic waves experience some sort of strong scattering at frequencies close to those of the boson peak and thus explain the existence of the plateau region in the thermal conductivity of glasses at $\sim$10 K. Moreover, a correlation has been proposed between the energy position of the boson peak and this region of strong scattering in glasses [28]. However, the observed rapid increase of $\Gamma(q)$ with q or, more precisely, with Ω, can be nowadays expected in quite different frameworks, e.g.: (i) lattice models with force-constant disorder [29,31], or continuum models with spatially fluctuating elastic constants [33], where it is basically a harmonic phenomenon; (ii) models that assume an anharmonic coupling between sound waves and weakly interacting quasilocal modes as the soft potential model [32], where anharmonicity clearly plays a direct role. It is then clear that more information from the experimental side is needed in order to discriminate among different models.

4.2. Relaxation processes in liquids

The susceptibility spectrum of a liquid system in response to an external perturbation is generally smooth and characterized by broad peaks. These peaks correspond to relaxation processes which dump the perturbation applied to the system. Among the various relaxation processes which characterize the dynamical response of a liquid to a given perturbation, there is one which plays a particularly important role since it is universal – it is present in all liquids and dense fluids at basically the same frequency independently of the perturbation which is applied: this is the structural, or α, relaxation process. Its name derives from the fact that it is believed to be related to the collective structural rearrangement of groups of atoms or molecules in response to an external perturbation (or to local fluctuations). The position ω_α of the structural relaxation peak in the loss spectra defines a characteristic time, $\tau = \omega_\alpha^{-1}$. This characteristic time is strongly temperature dependent, being generally proportional to the shear viscosity as

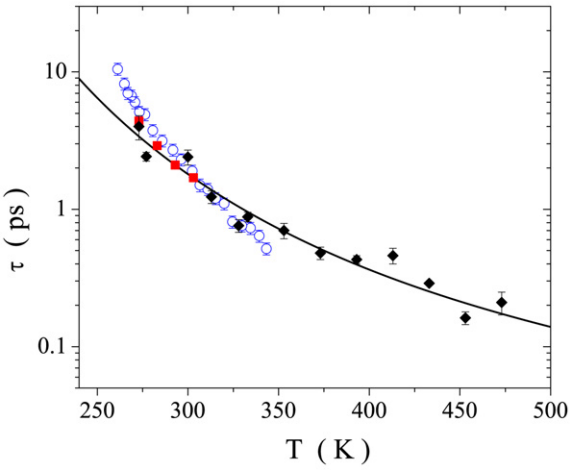

Fig. 6. Temperature dependence of the relaxation time τ of liquid water kept at ≈ 1 g/cm^3 density: IXS results (filled diamonds) [45] are compared to ultrasound data (filled squares) [46] and to inelastic ultraviolet radiation scattering data (open circles) [47]. The full line describes an Arrhenius behavior with an activation energy of 3.8 kcal/mol that well represents the data at high temperature but fails at low temperature.

$\tau \approx \eta_s / G_\infty$, where η_s is the shear viscosity and G_∞ is the limiting shear modulus. It follows that $\tau \sim 1$ ps for ordinary liquids with a viscosity of the order of 10^{-3} Pa s and $\sim$1000 s at the glass transition temperature – for those liquids that can reach it – where the viscosity is $\sim 10^{12}$ Pa s.

The intervention of the structural relaxation in the dynamical response of a liquid can be rationalized by viscoelastic models. These models basically describe the obvious kinetic result that if a liquid is studied on a time scale much longer than τ, one probes its equilibrium, or viscous, properties; and if a liquid is studied on a time scale much shorter than τ, one probes its out-of-equilibrium, or elastic, properties. The temperature at which this viscoelastic transition is located obviously depends on the frequency ω used to probe the system and is defined by the condition $\omega\tau(T) = 1$. This clarifies that, while low-frequency techniques are needed to probe the viscoelastic properties of glass-formers close to the glass transition temperature, high-frequency probes are required to perform such studies in liquids at ordinary conditions. This is for example the case of water at room temperature, and of a wide class of other liquids, where techniques exploring the THz frequency range are needed. This, in turn, explains and justifies the success of IXS in this kind of studies. Fig. 6 reports, as an example, the comparison of τ values as determined in an IXS experiment on liquid water kept at $\approx$1 g/cm^3 density [45] with both ultrasound data [46] and with results recently obtained using inelastic ultraviolet radiation scattering [47]. Fig. 6 clarifies that while IXS is the only probe that provides reliable τ values in water at high temperature, it becomes less and less sensitive on decreasing the temperature as the structural relaxation leaves the IXS frequency window.

IXS studies of the structural relaxation in liquids are interesting for several reasons. One reason is that they give the possibility to probe this relaxation up to the highest possible frequencies where it can be detected. Above the THz frequency range, in fact the relaxation of an applied perturbation will more likely occur through different paths. Another source of interest for these studies is that they give an idea of the q value up to which it is still possible to make use of the continuum hypothesis inherent in the hydrodynamics description of the density–density correlation function of a liquid. In the case of water, for example, the macroscopic hydrodynamics description is still meaningful up to $q \sim 2$ nm^{-1} [45], which is a fairly large value. The same result can be rephrased by saying that the atomic dynamics in water shows a homogeneous character down to a length scale of $\approx$30 Å. It is important to emphasize that this result is not specific to water but applies in general to simple liquids [48–50].

Besides the structural relaxation, the microscopic relaxation has also been characterized in some detail in IXS experiments [48,49,51]. This relaxation is formally related to the dephasing of the different Fourier q-components of the normal modes of vibration in the disordered liquid structure. The characteristic time associated to this relaxation channel has been characterized in one favourable case, and has been found to be in the 0.1–0.01 ps range [48], thus faster then – though not completely decoupled from – the structural relaxation. In supercritical conditions, the microscopic relaxation has been found to have a collisional nature [51].

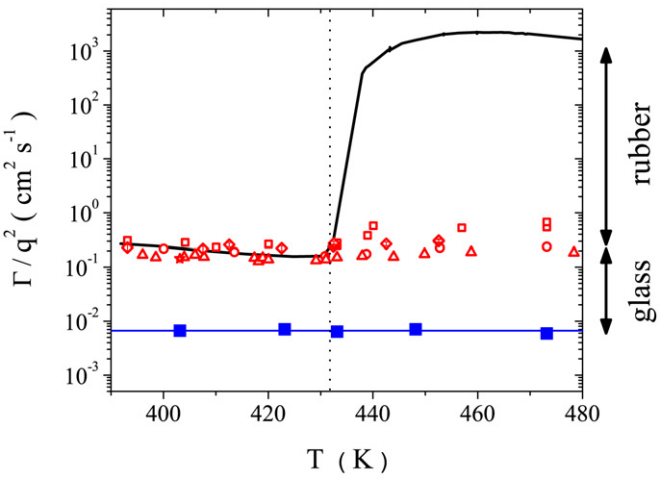

Fig. 7. Temperature dependence of the acoustic absorption in liquid sulfur reported as Γ/q^2. The IXS results (filled squares) refer to the 0.4–1.1 THz frequency range [56]. Ultrasound data from Refs. [54,55] (open circles), Ref. [52] (open squares) and Ref. [53] (open diamond) cover the 6–155 MHz frequency range. The difference between the IXS and ultrasound data corresponds to the glass transition that takes place in the frequency range comprised between 0.1 GHz and 1 THz. The full line is the zero-frequency, simple hydrodynamics prediction for Γ/q^2, from Refs. [56–58]. The dotted vertical line marks the λ-transition temperature at 432 K. The difference between the ultrasound data and the zero-frequency ones corresponds to the liquid to rubber transition that takes place at frequencies lower than 6 MHz and only in the high-temperature polymeric phase.

It is as well important to underline that the description of the high-frequency density-fluctuations dynamics in terms of two main relaxations – the structural and the microscopic one – seems to have general validity for simple enough liquids, having been verified in Van der Waals liquids [49] as well as in hydrogen-bonded liquids [50] and in liquid metals [48]. This is no longer true in liquids that present a more complex phenomenology, since their relaxation pattern will be more complex as well. For these cases, IXS experiments have proven to provide a valuable information as well when they are used to extend towards high frequencies the traditional acoustic studies performed in the MHz to GHz frequency range.

An example of that is provided by the case of liquid sulfur. In fact, sulfur undergoes, at 432 K and room pressure, a reversible so-called λ-transition between a molecular liquid composed of S_8 rings and a complex solution of polymeric chains in S_8 monomers. In particular, ultrasound studies [52–55] of this liquid–liquid transition had left open the question of whether the high-temperature polymeric liquid form of sulfur could be considered a viscoelastic system at all, and what would be the relaxation channels that mirror the λ-transition in the dynamical properties. A recent IXS study [56], see Fig. 7, has provided high frequency acoustic data that have clarified that viscoelasticity is indeed present in this peculiar liquid phase though it appears under a more complex form than in simple liquids. Specifically, the atomic dynamics relaxes in two main steps in time (or frequency):

(i) A first step can be associated to the structural relaxation and is common to both sulfur liquids. In the temperature range around the λ-transition temperature, this relaxation takes place on the 10 ps time scale and reflects both the relative motion of the chain segments between entanglement loci and the solvent molecules dynamics.
(ii) A second, slower step corresponds to the slippage of the entanglement loci so that the configurational rearrangements of segments separated by entanglements can then take place. This relaxation characterizes the high-temperature polymeric phase, is strongly temperature dependent and takes place on the 10 ms time scale close to the transition temperature.

This phenomenology can be summarized by saying that the first relaxation step describes the glass transition observed as a function of frequency, while the second relaxation step corresponds to a liquid-rubber transition observed only in the polymeric liquid as a function of frequency. The existence of a rubbery plateau in the polymeric liquid phase of sulfur clarifies that it basically behaves as an uncross-linked solution of high molecular weight polymers.

4.3. The non-ergodicity factor

The quasi-elastic peak present in the atomic $S(q, E)$ spectra of disordered systems holds some very interesting information which complements/extends that which can be obtained from the study of the acoustic excitations. In an undercooled liquid and in a glass, the quasi-elastic peak width – being proportional to the inverse of the structural relaxation time – is very narrow as compared to the typical energy resolution function of an IXS experiment, and cannot be measured. Its area, however, is readily determined and – once normalized to the static structure factor $S(q)$ – gives the so-called effective non-ergodicity factor f_q – a central quantity in the mode-coupling description of the liquid-to-glass transition [59]. In its basic version, this theory deals with the dynamics of density fluctuations in the early stage of supercooling, and the glass transition is described as an ergodic to non-ergodic transition occurring at a critical temperature T_c and signaled by a singular behavior of the long-time limit of the normalized density correlator – the non-ergodicity factor. A zero value of the non-ergodicity factor means that a given particle will eventually escape, on a long enough timescale, from the cage of its nearest neighbors, and the system is ergodic. A finite value of the non-ergodicity factor, conversely, corresponds to a frozen structural relaxation which prevents the particles to escape their cages. Thus, the non-ergodicity factor is zero in the liquid phase but positive in the glassy state, and it changes discontinuously as the temperature crosses T_c. The effective non-ergodicity parameter which is measured in scattering experiments corresponds to the normalized density correlator calculated not at $t = \infty$ but at $t = \hbar/\Delta E$, where ΔE is the experimental energy resolution. The effective non-ergodicity factor is expected to show the same discontinuity as the non-ergodicity factor. However, while it equals the non-ergodicity factor in the non-ergodic phase, it is expected to keep a non-zero value in the ergodic phase across T_c. Specifically, the peculiar temperature and wavevector dependences expected for f_q are [59]: (i) A square-root temperature behavior below T_c, $f_q(T) = f_q^c + h_q\sqrt{(T_c - T)/T_c}$, where f_q^c is the critical non-ergodicity parameter and h_q the critical amplitude at a fixed wavevector q; (ii) A dependence on q of f_q^c and of h_q which are in phase and in anti-phase with the static structure factor $S(q)$, respectively. In the last two decades both the peculiar T and q behavior of the non-ergodicity factor predicted by the mode-coupling theory have been tested in Van-der-Waals molecular liquids. The situation is much less clear for associated and covalent liquids, the ubiquitous class of liquids including water and silica. In these liquids the local order extends over several neighboring molecules, often giving rise to a non-trivial q behavior of the static structure factor, and the available results of experimental investigations are often mutually contradictory.

A recent IXS experiment [60] has provided experimental evidence that hydrogen bond clustering can coexist with the signature of the ergodic to non-ergodic transition predicted by the mode-coupling theory for simple liquids, see Fig. 8. The system investigated, m-toluidine, is characterized by a spatial organization of the molecules induced by hydrogen bonds extending over several molecular diameters and giving rise to nanometer size clusters.

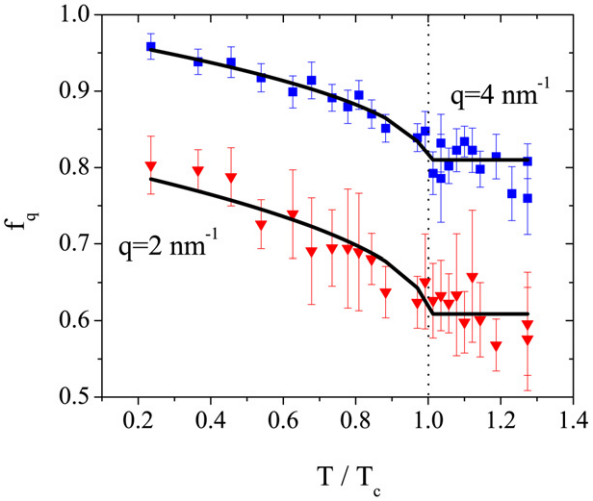

Fig. 8. Temperature dependence of the effective non-ergodicity factor f_q of m-toluidine for two different values of the exchanged wavevector q, from Ref. [60]. The temperature scale has been expressed in terms of the critical temperature $T_c = 230$ K. The solid lines are the best fits obtained using the square-root function predicted by the mode-coupling theory [59].

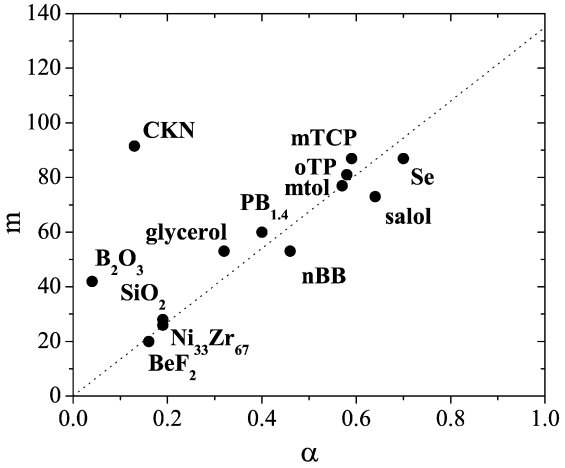

Fig. 9. Correlation between the parameter α describing the low-temperature behavior of the non-ergodicity factor and the kinetic fragility m. The original data set from Ref. [62] has been completed with the data for CKN and B_2O_3 [63,64] and for $Ni_{33}Zr_{67}$ [65,66].

The non-ergodicity factor is also related to the glass formation process in an additional subtle way through the concept of *fragility* [61]. Specifically, the kinetic fragility, m, is defined in terms of the shear viscosity η_s as:

$$m = \lim_{T \to T_g} \frac{\mathrm{d}\log(\eta_s)}{\mathrm{d}(T_g/T)},$$

where T_g is the glass transition temperature. Therefore, m is an index of how fast the shear viscosity increases on approaching the structural arrest at T_g. One interest in this classification lies in the attempt to relate the temperature behavior of a macroscopic transport property as η_s close to T_g to the microscopic interaction driving the dynamics of the system. In fact, the value of the fragility is empirically related to the kind of interaction potential among the particles constituting the system. Prototypical examples of fragile liquids are those composed by units interacting via isotropic bonds, such as Van der Waals-like molecular liquids. The strong glass-forming liquids, on the other hand, are those characterized by strong covalent directional bonds that form space filling networks. Hydrogen bonded systems are often called 'intermediate' between strong and fragile liquids.

A recent IXS study [62], see Fig. 9, has shown that, starting from the determination of the non-ergodicity factor in the low temperature glass, it is possible to identify a parameter that controls how fast the non-ergodicity factor decreases on increasing the temperature, and this turns out to be proportional to the fragility m. Specifically, the temperature dependence of f_q at low temperatures can be well described within the harmonic approximation for the vibrational dynamics of the glass; its inverse, f_q^{-1}, depends linearly on temperature and the slope of this line, α, is directly proportional to the fragility index of the glass. At a first glance, this result defines a new way to determine the fragility of a system starting from its glassy phase, microscopic properties. However, its real interest lies in the following observation. If we recall that: (i) the fragility is related to the temperature dependence of the viscosity on approaching T_g, and thus mirrors the diffusive properties of the system; and (ii) the non-ergodicity factor is only related to the vibrational properties of the harmonic glassy dynamics, we have to deduce that in a glass the vibrational properties below T_g are related to the diffusive properties above T_g [62]. Though in the meanwhile a couple of exceptions to the neat correlation between the low-temperature behavior of the non-ergodicity factor and the fragility index have been found [64], this result is still very fascinating and will require further studies to be fully understood.

5. Conclusions

The inelastic x-ray scattering technique has given an important contribution over the last ten years to our understanding of the high-frequency dynamics in liquids and glasses. It is now clear that acoustic-like excitations in disordered systems are present up to a relevant fraction of the first pseudo Brillouin zone size and show a crystal-like behavior [34]. At the same time, the damping of these excitations increases roughly as Ω^2, i.e. much faster than the characteristic energy of the excitations themselves which then become quite soon overdamped.

For both liquids and glasses, however, the most relevant information contained in the measured $S(q, E)$ spectra lies in the lower portion of the (q, E) range probed by IXS, say $q \leqslant 2$ nm^{-1} and $E \leqslant 5$ meV. For liquids, this is the range where simple hydrodynamics still holds, which leaves a reference of fundamental importance for any further interpretation of the IXS spectra [45]. In glasses, this is the relevant range where the acoustic excitations are strongly scattered [28], giving rise to some universal properties found in the low-temperature behavior of specific heat and thermal conductivity of glasses. Unfortunately this most interesting (q, E) range remains difficult for IXS studies mainly due to the present limitations in terms of energy resolution. However, the strong scientific case to push IXS studies of disordered systems towards lower and lower energies and wavenumbers is stimulating the development of new optical schemes to overcome the limitations of the technique. Promising schemes are now available [5], and the near future will hopefully see the advent of advanced IXS spectrometers pushing down the lowest reachable q and E values by as much as one decade.

Acknowledgements

C. Alba Simionesco, R. Angelini, G. Baldi, R. Bellissent, F. Bencivenga, L. Börjesson, S. Caponi, A. Chumakov, L. Comez, S. Corezzi, E. Courtens, L. Crapanzano, W. Crichton, A. Cunsolo, D. Fioretto, A. Fontana, M. Foret, V. Giordano, P. Giura, M. Krisch, C. Masciovecchio, A. Matic, M. Mezouar, A. Monaco, K. Niss, E. Pontecorvo, B. Rufflé, G. Ruocco, B. Ruta, B. Ruzicka, F. Scarponi, T. Scopigno, F. Sette, R. Vacher and R. Verbeni are gratefully acknowledged for a number of discussions on the issues presented here.

References

[1] B. Dorner, E. Burkel, T. Illini, J. Peisl, Z. Phys. B 69 (1987) 179.
[2] R. Verbeni, F. Sette, M.H. Krisch, U. Bergmann, B. Gorges, C. Halcoussis, K. Martel, C. Masciovecchio, J.F. Ribois, G. Ruocco, H. Sinn, J. Synchrotron Rad. 3 (1996) 62.
[3] C. Masciovecchio, U. Bergmann, M. Krisch, G. Ruocco, F. Sette, R. Verbeni, Nucl. Instr. Meth. B 111 (1996) 181.
[4] C. Masciovecchio, U. Bergmann, M. Krisch, G. Ruocco, F. Sette, R. Verbeni, Nucl. Instr. Meth. B 117 (1996) 339.
[5] Y. Shvyd'ko, X-Ray Optics, Springer-Verlag, 2004.
[6] M. Krisch, J. Raman Spectrosc. 34 (2003) 628.
[7] http://www.esrf.fr/UsersAndScience/Experiments/HRRS/ID16/.
[8] H. Sinn, E.E. Alp, A. Alatas, J. Barraza, G. Bortel, E. Burkel, D. Shu, W. Sturhahn, J.P. Sutter, T.S. Toellner, J. Zhao, Nucl. Instrum. Methods A 467–468 (2001) 1545.
[9] A.Q.R. Baron, Y. Tanaka, S. Goto, K. Takeshita, T. Matsushita, T. Ishikawa, J. Phys. Chem. Solids 61 (2000) 461.
[10] J.P. Boon, S. Yip, Molecular Hydrodynamics, Dover Publications Inc., New York, 1991.
[11] U. Balucani, M. Zoppi, Dynamics of the Liquid State, Clarendon Press, Oxford, 1994.
[12] R. Zwanzig, in: W. Brittin (Ed.), in: Lectures in Theoretical Physics, vol. 3, Wiley-Interscience, New York, 1961, pp. 106–141; H. Mori, Progr. Theor. Phys. 33 (1965) 423.
[13] W. Götze, in: J.P. Hansen, D. Levesque, J. Zinn-Justin (Eds.), Liquids, Freezing and the Glass Transition, North-Holland, Amsterdam, 1991, pp. 289–503.
[14] D. Levesque, L. Verlet, J. Kürkijarvi, Phys. Rev. A 7 (1973) 1690.
[15] G. Harrison, The Dynamic Properties of Supercooled Liquids, Academic Press, 1976.
[16] K.F. Herzfeld, T.A. Litovitz, Absorption and Dispersion of Ultrasonic Waves, Academic Press, New York, 1959.
[17] F. Sette, G. Ruocco, M. Krisch, C. Masciovecchio, R. Verbeni, U. Bergmann, Phys. Rev. Lett. 77 (1996) 83.
[18] M. Sampoli, G. Ruocco, F. Sette, Phys. Rev. Lett. 79 (1997) 1678.
[19] T. Scopigno, E. Pontecorvo, R. Di Leonardo, M. Krisch, G. Monaco, G. Ruocco, B. Ruzicka, F. Sette, J. Phys.: Condens. Matter 15 (2003) S1269.
[20] B. Ruzicka, T. Scopigno, S. Caponi, A. Fontana, O. Pilla, P. Giura, G. Monaco, E. Pontecorvo, G. Ruocco, F. Sette, Phys. Rev. B 69 (2004) 100201(R).
[21] E. Pontecorvo, M. Krisch, A. Cunsolo, G. Monaco, A. Mermet, R. Verbeni, F. Sette, G. Ruocco, Phys. Rev. E 71 (2005) 011501.
[22] Amorphous solids: low-temperature properties, in: W.A. Phillips (Ed.), Springer-Verlag, Berlin, 1981.
[23] U. Buchenau, N. Nücker, A.J. Dianoux, Phys. Rev. Lett. 53 (1984) 2316.
[24] S.R. Elliott, Physics of Amorphous Materials, Longmans, New York, 1990.
[25] W.A. Phillips, J. Low Temp. Phys. 7 (1972) 351.
[26] P.W. Anderson, B.I. Halperin, C.M. Varma, Philos. Mag. 25 (1972) 1.
[27] F. Sette, M.H. Krisch, C. Masciovecchio, G. Ruocco, G. Monaco, Science 280 (1998) 1550.
[28] B. Rufflé, G. Guimbretière, E. Courtens, R. Vacher, G. Monaco, Phys. Rev. Lett. 96 (2006) 045502; See also G. Ruocco, A. Matic, T. Scopigno, S.N. Yannopoulos, Phys. Rev. Lett. 98 (2007) 079601; B. Rufflé, G. Guimbretière, E. Courtens, R. Vacher, G. Monaco, Phys. Rev. Lett. 98 (2007) 079602.

[29] W. Schirmacher, G. Diezemann, C. Ganter, Phys. Rev. Lett. 81 (1998) 136.
[30] L. Angelani, M. Montagna, G. Ruocco, G. Viliani, Phys. Rev. Lett. 84 (2000) 4874.
[31] S.N. Taraskin, Y.L. Loh, G. Natarajan, S.R. Elliott, Phys. Rev. Lett. 86 (2001) 1255.
[32] V.L. Gurevich, D.A. Parshin, H.R. Schober, Phys. Rev. B 67 (2003) 094203.
[33] W. Schirmacher, Europhys. Lett. 73 (2006) 892.
[34] G. Ruocco, F. Sette, J. Phys.: Condens. Matter 13 (2001) 9141.
[35] M. Foret, R. Vacher, E. Courtens, G. Monaco, Phys. Rev. B 66 (2002) 024204.
[36] A.F. Ioffe, A.R. Regel, Prog. Semicond. 4 (1960) 237.
[37] P. Benassi, M. Krisch, C. Masciovecchio, V. Mazzacurati, G. Monaco, G. Ruocco, F. Sette, R. Verbeni, Phys. Rev. Lett. 77 (1996) 3835.
[38] C. Masciovecchio, V. Mazzacurati, G. Monaco, G. Ruocco, T. Scopigno, F. Sette, P. Benassi, A. Cunsolo, A. Fontana, M. Krisch, A. Mermet, M. Montagna, F. Rossi, M. Sampoli, G. Signorelli, R. Verbeni, Philos Mag. B 79 (1999) 2013.
[39] O. Pilla, A. Cunsolo, A. Fontana, C. Masciovecchio, G. Monaco, M. Montagna, G. Ruocco, T. Scopigno, F. Sette, Phys. Rev. Lett. 85 (2000) 2136.
[40] C. Masciovecchio, A. Mermet, G. Ruocco, F. Sette, Phys. Rev. Lett. 85 (2000) 1266.
[41] G. Ruocco, F. Sette, R. Di Leonardo, D. Fioretto, M. Lorentzen, M. Krisch, C. Masciovecchio, G. Monaco, F. Pignon, T. Scopigno, Phys. Rev. Lett. 83 (1999) 5583.
[42] G. Ruocco, F. Sette, R. Di Leonardo, G. Monaco, M. Sampoli, T. Scopigno, G. Viliani, Phys. Rev. Lett. 84 (2000) 5788.
[43] W. Schirmacher, G. Ruocco, T. Scopigno, Phys. Rev. Lett. 98 (2007) 025501.
[44] B. Rufflé, M. Foret, E. Courtens, R. Vacher, G. Monaco, Phys. Rev. Lett. 90 (2003) 095502.
[45] G. Monaco, A. Cunsolo, G. Ruocco, F. Sette, Phys. Rev. E 60 (1999) 5505.
[46] W.M. Slie, A.R. Donfor Jr., T.A. Litivitz, J. Chem. Phys. 44 (1966) 3712.
[47] C. Masciovecchio, S.C. Santucci, A. Gessini, S. Di Fonzo, G. Ruocco, F. Sette, Phys. Rev. Lett. 92 (2004) 255507.
[48] T. Scopigno, U. Balucani, G. Ruocco, F. Sette, Phys. Rev. Lett. 85 (2000) 4076.
[49] A. Cunsolo, G. Pratesi, R. Verbeni, D. Colognesi, C. Masciovecchio, G. Monaco, G. Ruocco, F. Sette, J. Chem. Phys. 114 (2001) 2259.
[50] R. Angelini, P. Giura, G. Monaco, G. Ruocco, F. Sette, R. Verbeni, Phys. Rev. Lett. 88 (2002) 255503.
[51] F. Bencivenga, A. Cunsolo, M. Krisch, G. Monaco, L. Orsingher, G. Ruocco, F. Sette, A. Vispa, Phys. Rev. Lett. 98 (2007) 085501.
[52] A.W. Pryor, E.G. Richardson, J. Phys. Chem. 59 (1955) 14.
[53] J.L. Hunter, T.L. Francavilla, J. Acoust. Soc. Am. 35 (1963) 1834.
[54] V.F. Kozhevnikov, J.M. Viner, P.C. Taylor, Phys. Rev. B 64 (2001) 214109.
[55] V.F. Kozhevnikov, W.B. Payne, J.K. Olson, C.L. McDonald, C.E. Inglefield, J. Chem. Phys. 121 (2004) 7379.
[56] G. Monaco, L. Crapanzano, R. Bellissent, W. Crichton, D. Fioretto, M. Mezouar, F. Scarponi, R. Verbeni, Phys. Rev. Lett. 95 (2005) 255502.
[57] R.F. Bacon, R. Fanelli, J. Am. Chem. Soc. 65 (1943) 639.
[58] K.M. Zheng, S.C. Greer, J. Chem. Phys. 96 (1992) 2175.
[59] W. Götze, L. Sjögren, Rep. Prog. Phys. 55 (1992) 241.
[60] L. Comez, S. Corezzi, G. Monaco, R. Verbeni, D. Fioretto, Phys. Rev. Lett. 94 (2005) 155702.
[61] C.A. Angell, J. Non-Crys. Solids 131–133 (1991) 13.
[62] T. Scopigno, G. Ruocco, F. Sette, G. Monaco, Science 302 (2003) 849.
[63] A. Matic, L. Börjesson, G. Ruocco, C. Masciovecchio, A. Mermet, F. Sette, R. Verbeni, Europhys. Lett. 54 (2001) 77.
[64] V.N. Novikov, Y. Ding, A.P. Sokolov, Phys. Rev. E 71 (2005) 061501.
[65] T. Scopigno, J.-B. Suck, R. Angelini, F. Albergamo, G. Ruocco, Phys. Rev. Lett. 96 (2006) 135501;
See also E. Courtens, M. Foret, B. Rufflé, R. Vacher, Phys. Rev. Lett. 98 (2007) 079603;
T. Scopigno, R. Angelini, G. Ruocco, J.-B. Suck, Phys. Rev. Lett. 98 (2007) 079604.
[66] M. Guerdane, Ph.D. thesis, University of Göttingen, Göttingen, 2000.